JACS
JOURNAL OF THE AMERICAN CHEMICAL SOCIETY

Communication

pubs.acs.org/JACS

A Catalytic Path for Electrolyte Reduction in Lithium-Ion Cells Revealed by *in Situ* Attenuated Total Reflection-Fourier Transform Infrared Spectroscopy

Feifei Shi,[†,§] Philip N. Ross,[§] Hui Zhao,[∥] Gao Liu,[∥] Gabor A. Somorjai,*[,‡,§] and Kyriakos Komvopoulos*[,†]

[†]Department of Mechanical Engineering and [‡]Department of Chemistry, University of California, Berkeley, California 94720, United States

[§]Materials Sciences Division and [∥]Environmental Energy Technologies Division, Lawrence Berkeley National Laboratory, Berkeley, California 94720, United States

Supporting Information

ABSTRACT: Although controlling the interfacial chemistry of electrodes in Li-ion batteries (LIBs) is crucial for maintaining the reversibility, electrolyte decomposition has not been fully understood. In this study, electrolyte decomposition on model electrode surfaces (Au and Sn) was investigated by *in situ* attenuated total reflection-Fourier transform infrared (ATR-FTIR) spectroscopy. Simultaneously obtained ATR-FTIR spectra and cyclic voltammetry measurements show that lithium ethylene dicarbonate and lithium propionate form on the Au electrode at 0.6 V, whereas diethyl 2,5-dioxahexane dicarboxylate and lithium propionate form on the Sn electrode surface at 1.25 V. A noncatalytic reduction path on the Au surface and a catalytic reduction path on the Sn surface are introduced to explain the surface dependence of the overpotential and product selectivity. This represents a new concept for explaining electrolyte reactions on the anode of LIBs. The present investigation shows that catalysis plays a dominant role in the electrolyte decomposition process and has important implications in electrode surface modification and electrolyte recipe selection, which are critical factors for enhancing the efficiency, durability, and reliability of LIBs.

Rechargeable lithium-ion batteries (LIBs) are widely used in energy storage, portable electronics, and electric vehicles.[1] It is well-known that the electrolyte of LIBs is thermodynamically unstable in the operating potential range, i.e., the electrolyte is reduced and oxidized on the anode and cathode surfaces, respectively. The decomposed electrolyte forms a film on the electrode surfaces, referred to as the solid-electrolyte interphase (SEI), which passivates the electrodes, inhibiting further parasitic reactions while allowing the conduction of the Li^+ ions. Because of the significant impact on the stability and durability of LIBs,[2] the composition, properties, and formation mechanism of SEI on inactive (e.g., Au),[3,4] active (e.g., Li),[5] and carbon[6] electrodes have been studied extensively. SEI components include both carbonaceous (e.g., $(CH_2OCO_2Li)_2$, $ROCO_2Li$, Li_2CO_3, and polycarbonates) and noncarbonaceous (e.g., LiF, Li_2O, and LiOH) compounds.[7−10] However, because most of the aforementioned studies used *ex situ* techniques, the reported results have inevitably been compromised due to the electrolyte residue, operation uncertainty, and air sensitivity of the SEI.[11] To better understand the electrolyte decomposition process and growth mechanism of the SEI, it is necessary to perform *in situ* studies of the electrode−electrolyte interface.

Previous studies have indicated that the formation mechanism and composition of the SEI greatly depend on the type of electrolyte and additive used.[7,12] It was postulated that cyclic carbonate (e.g., ethylene carbonate (EC)) dominates the primary Li^+ solvation sheath and ultimately most of the reduction product is a signature of the cyclic carbonate reduction by an electron transfer reaction. However, recent studies[13−15] have shown a surface dependence of both reduction potentials and products, suggesting that electrochemical reduction of the electrolyte solvent is an electrocatalytic process with kinetics strongly dependent on the electrode material.[16] Therefore, a thorough understanding of the roles of the primary Li^+ ion solvation structure and electrode material on the electrolyte decomposition process is essential.

An *in situ* attenuated total reflection-Fourier transform infrared (ATR-FTIR) spectroscopy approach (see Supporting Information (SI) for details) was developed and used to systematically study the electrolyte reduction process. Considering the complexity of surface functional groups on real battery electrodes, two simple model electrode materials were chosen for study, namely Au as a metal electrode without any functional groups and Sn as an electrode material with oxygen functional groups, which can be controlled and/or identified.[17−20] As a noble metal, Au is relatively inert and weakly interacts with aprotic electrolyte solvent, whereas Sn forms a native oxide layer upon exposure to the atmosphere, causing a catalytic effect on many reactions, including electrocatalytic reactions.[17]

Figure 1a and 1b show cyclic voltammograms (CVs) of Au and Sn electrodes in 1 M $LiPF_6$ electrolyte (EC/DEC = 1:2 v/v). The potential was swept from 2 to 0 V (all potentials are referred to the Li/Li^+ redox couple) at a scan rate of 1 mV/s. On the Au electrode, besides the features associated with underpotential deposition of Li below 0.2 V and the two anodic peaks at ∼0.3 and ∼0.5 V corresponding to Li dissolution, a reduction (cathodic) peak of −25 $\mu A/cm^2$ is observed at ∼0.6 V in the

Received: December 17, 2014
Published: February 17, 2015

DOI: 10.1021/ja5128456
J. Am. Chem. Soc. 2015, 137, 3181−3184

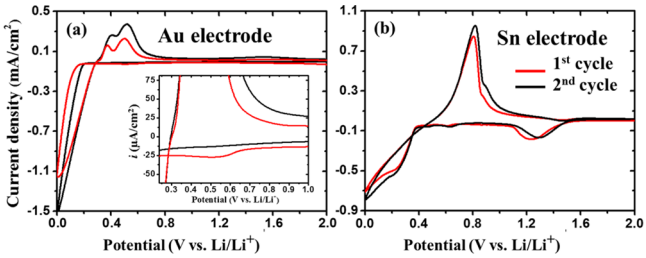

Figure 1. Cyclic voltammograms of (a) Au and (b) Sn electrodes in 1 M $LiPF_6$ electrolyte (EC/DEC = 1:2 v/v) for 1 mV/s scan rate. The inset in (a) is a magnified plot of the CV region revealing the formation of SEI.

first cycle but not in the second cycle (see inset of Figure 1a).[4,21] The disappearance of this peak in the second cycle is attributed to the formation of a stable reduction product, which passivates the surface from further electrolyte reduction. Conversely, on the Sn electrode, besides the features below ~0.5 V associated with Sn lithiation and the features above 0.5 V in the anodic sweep indicating Sn delithiation, a reduction peak consistently appears at ~1.25 V, indicating that the reduction products do not passivate the electrode surface from further electrolyte reduction after lithiation and delithiation.[13,14] Considering the identical experimental conditions, the different electrolyte reduction potentials reveal different reactions on each electrode material.

In situ ATR-FTIR spectroscopy was used to study the surface chemistry associated with these different reaction paths on the Au and Sn electrodes. Experimental details of the ATR-FTIR studies can be found in the SI. The electrode potential was changed from the open circuit potential (OCP) to various potentials before Li deposition and held at each potential for 2 h while spectra were acquired. Figure 2a and 2b show the potential dependence of *in situ* ATR-FTIR spectra of Au and Sn electrodes, respectively, in EC/DEC 1 M $LiPF_6$ electrolyte. The dashed lines indicate the new peaks encountered at different potentials. The spectrum of the EC/DEC 1 M $LiPF_6$ electrolyte at OCP is similar to that obtained in previous studies;[22−24] more details about the peak assignment are provided in the SI (Figure S3 and Table S1). Five new peaks (2920, 2851, 1576, 1557, and 1115 cm^{-1}) appear in the spectrum of the Au electrode at 0.6 V potential, which is the electrolyte reduction potential, as shown by the CV of the Au electrode (Figure 1a). These peaks are assigned to lithium ethylene dicarbonate (LiEDC) (1115 cm^{-1}) and lithium propionate (2920, 2851, and 1565 cm^{-1}). The spectrum of the sodium propionate (Figure 2c) indicates that the doublet peak at 1576 and 1557 cm^{-1} in the *in situ* ATR-FTIR spectra (Figure 2a and 2b) is due to the formation of lithium propionate (peak at 1565 cm^{-1}). The splitting of the peak at 1565 cm^{-1} (pure lithium propionate) to a doublet peak (1576 and 1557 cm^{-1}) is due to the solvation of EC, as explained in the SI (Figure S4). The C═O stretch at 1663 cm^{-1} corresponding to LiEDC is not visible in the spectrum shown in Figure 2a under the strong background signal of the electrolyte. The peaks at 1663 and 1115 cm^{-1} are assigned to the C═O stretch and the C−O−C stretch of the dimer format of LiEDC, respectively.[25] In addition, the intensity of the C═O stretch is very sensitive to its association in the salt, e.g., dimer versus monomer. Thus, the absence of the 1663 cm^{-1} peak is attributed to the different association structure of the LiEDC on the electrode surface. Alternatively, the C═O stretch is observed in the *ex situ* ATR-FTIR results presented below (in these tests most of the bulk electrolyte was rinsed off). New features are also observed in the spectra of the Sn electrode (Figure 2b), but in a higher potential range compared to the Au

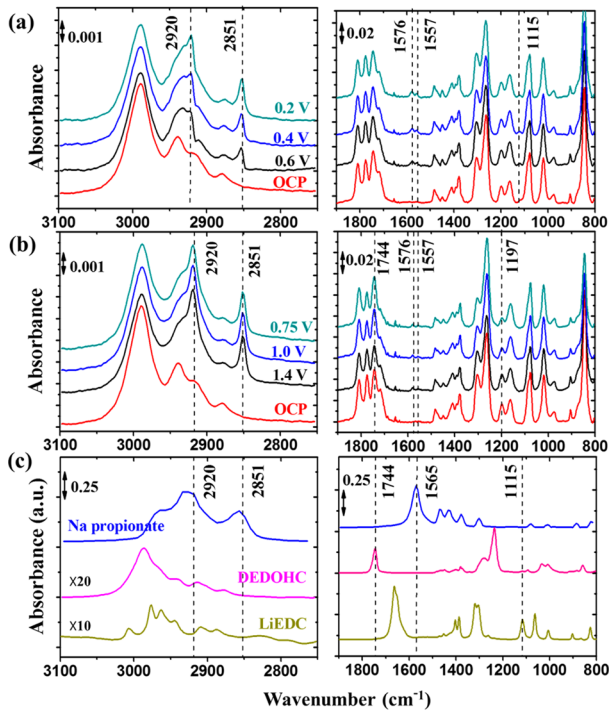

Figure 2. *In situ* ATR-FTIR spectra of (a) Au electrode obtained after applying a potential of open circuit potential (OCP), 0.6, 0.4, and 0.2 V and (b) Sn electrode obtained after applying a potential of OCP, 1.4, 1.0, and 0.75 V (both electrodes are in EC/DEC 1 M $LiPF_6$ electrolyte). (c) ATR-FTIR spectra of sodium propionate (reference spectrum for lithium propionate), DEDOHC, and LiEDC.

electrode. The peaks at 2920, 2851, 1576, and 1557 cm^{-1} observed at a potential of 1.4 V are assigned to lithium propionate, whereas the peak at 1744 cm^{-1} is assigned to diethyl 2,5-dioahexane dicarboxylate (DEDOHC). Because the FTIR spectra of DEDOHC and DEC are similar, reference spectra (Figure S5, SI) were used to validate the assignment of the peak at 1744 cm^{-1} to DEDOHC. Further details about the characterization of DEDOHC can be found elsewhere.[26] The intensity of the peak at 1197 cm^{-1} (assigned to the −C−O− stretch of Li-solvated EC) decreases with the potential concurrently with the formation of DEDOHC. A possible explanation is a change in the near-surface EC solvation state at these potentials. In brief, lithium propionate is identified as a reduction product on both Au and Sn electrodes, whereas the reduction products LiEDC and DEDOHC are detected only on the Au and Sn electrode surfaces, respectively. The presence of different chemical species is direct evidence that the electrode material exhibits a surface dependence on both the selectivity and overpotential of electrolyte reduction.

Many of the new features in the *in situ* ATR-FTIR spectra are barely observable above the background signal of the bulk electrolyte. Thus, to better resolve these features and determine which is associated with less soluble products, ATR-FTIR analysis was performed *ex situ* with a previously developed method.[27] *Ex situ* ATR-FTIR spectra were collected from electrodes subjected to the same experimental conditions (i.e., constant potential of 0.2 or 0.75 V applied for 2 h to the Au and Sn electrodes, respectively, both in EC/DEC 1 M $LiPF_6$ electrolyte). As expected, none of the features assigned to lithium propionate were observed *ex situ* because of its IR absorbance sensitivity and solubility in the rinsing solvent

DOI: 10.1021/ja5128456
J. Am. Chem. Soc. 2015, 137, 3181−3184

(dimethyl carbonate), which explains why this product is rarely reported in the literature. In the spectra shown in Figure 3, the

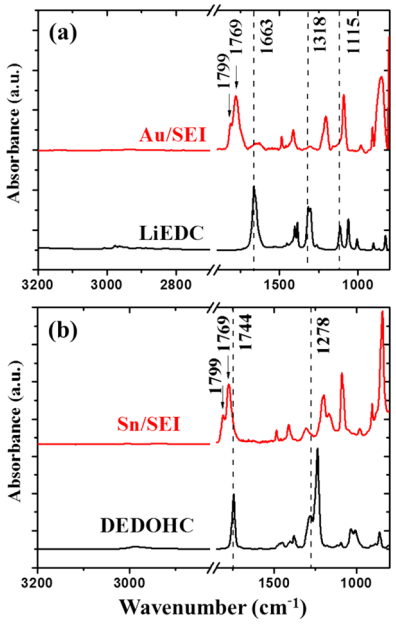

Figure 3. *Ex situ* ATR-FTIR spectra of (a) LiEDC and SEI formed on the Au electrode surface obtained after applying a constant potential of 0.2 V for 2 h; (b) DEDOHC and SEI formed on the Sn electrode surface obtained after applying a constant potential of 0.75 V for 2 h (both electrodes are in EC/DEC 1 M $LiPF_6$ electrolyte).

peaks at 1799 and 1769 cm^{-1} are assigned to the C═O stretch of EC in 1 M $LiPF_6$ electrolyte. The peaks at 1663 and 1318 cm^{-1} confirm the presence of LiEDC as a stable product precipitating on the Au electrode (thus, an SEI component), whereas the peaks at 1744 and 1278 cm^{-1} confirm the assignment of DEDOHC as a reduction product on the Sn electrode, consistent with the *in situ* results. Since the organic salts (e.g., LiEDC) are less soluble than the organic compounds (e.g., DEDOHC)[28,29] in the electrolyte, LiEDC precipitates on the Au electrode during the first cycle, preventing further decomposition of the electrolyte. In contrast, the Sn electrode is not passivated by the more soluble DEDOHC; therefore, electrolyte decomposition occurs in each cycle. This explains the CV curves shown in Figure 1a and 1b, which indicate that different products of catalysis forming on the Au and Sn electrodes may affect the SEI stability during cycling.

The CV curves and FTIR spectra of the Au and Sn surfaces show that both the overpotential and selectivity exhibit clear surface dependence during electrolyte reduction. The noncatalytic (Au) and catalytic (Sn) reduction paths shown in Scheme 1a and 1b, respectively, can be used to explain the overpotential and selectivity surface dependence. The EC molecular reduction potential is ~0.9 V vs Li/Li^+, which mainly depends on the solvation condition of EC.[30] The electrolyte reduction potential on the Au surface is equal to ~0.6 V, which is close to that of a graphite electrode (~0.75 V)[31] and lower than the theoretical value (0.9 V), suggesting that the reduction path on the Au surface is noncatalytic. On the contrary, the reduction potential on the Sn surface is much higher (~1.25 V), revealing a typical catalytic reduction process and can be attributed to the much stronger interaction of the Sn surface with the solvent molecules, which lowers the barrier for the subsequent electron

Scheme 1. Proposed Formation Mechanisms of Reduction Products[a]

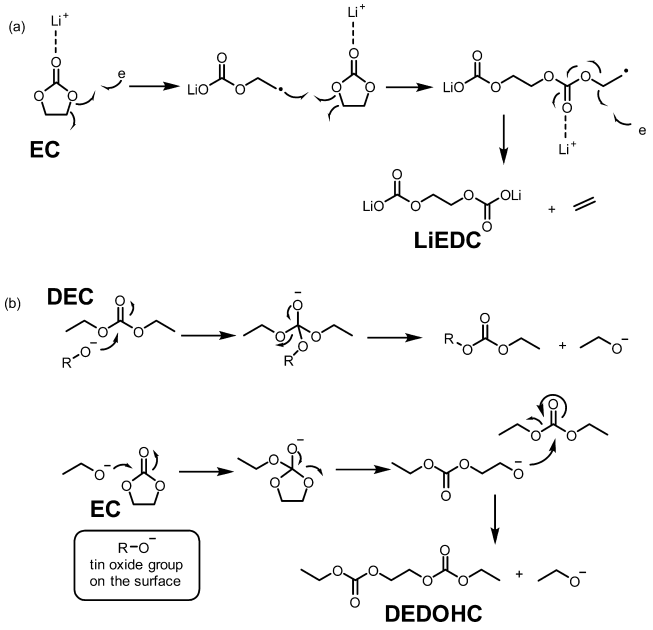

[a](a) A noncatalytic path leads to the formation of LiEDC on the Au electrode surface. The inactive electrode primarily serves as a current transfer medium; thus, the state of ion solvation is the dominant factor in the electrolyte decomposition process. (b) A catalytic path leads to the formation of DEDOHC on the Sn electrode surface. The active electrode surface strongly interacts with the cosolvent molecule DEC, whereas the effect of the ion solvation state is secondary; therefore, electrolyte reduction follows a catalytic path and the electrolyte decomposition demonstrates surface dependence.

transfer steps.[16] Furthermore, the reduction selectivity of the Au electrode differs from that of the Sn electrode. On the inactive Au surface, the main electrolyte reduction product is LiEDC, which, according to the "solvation sheath" argument,[7,12] is a signature EC-reduction product. Such product has also been found on graphite[31] and Ni[25] electrodes. As shown in Scheme 1a, in the absence of a strong interaction between the Au electrode and the electrolyte solvent, the solvated molecule is reduced by an electron, yielding the thermodynamically favorable product LiEDC. On the active Sn electrode, which is covered by oxygen species, the main reduction product is DEDOHC. As a transesterification compound of the electrolyte, the formation mechanism of DEDOHC has been systematically investigated.[32−35] The ethyl oxide radical is an important intermediate catalyst during the formation of DEDOHC. As shown in Scheme 1b, the strong interaction between DEC and Sn oxide produces ethyl oxide, which triggers the decomposition of EC and the formation of DEDOHC. Experimental validation of the above analysis can be found in the SI (Figures S6 and S7). To summarize, the electrolyte decomposition exhibits clear surface dependence. The inactive Au electrode barely interacts with the electrolyte solvent and the state of ion solvation mainly determines the electrolyte reduction; thus, the Au electrode primarily serves as current transfer medium and the electrolyte reduction follows a noncatalytic path. Conversely, the active Sn electrode strongly interacts with the solvent molecules and the state of ion solvation is secondary; thus, the Sn electrode serves as a catalyst and the electrolyte reduction follows a catalytic path.

DOI: 10.1021/ja5128456
J. Am. Chem. Soc. 2015, 137, 3181−3184

In conclusion, standard Li-ion electrolyte reduction on two metal electrode surfaces (Au and Sn) was investigated by *in situ* ATR-FTIR spectroscopy. A pronounced surface dependence of the overpotential and reduction products was observed in CV tests and confirmed by ATR-FTIR spectral analysis. It was found that relatively insoluble LiEDC forms on the Au electrode at ~0.6 V, whereas relatively soluble DEDOHC forms on the Sn electrode at ~1.25 V. As another reduction product, lithium propionate exists on both electrode surfaces. Two different reaction mechanisms were introduced to explain the observed surface dependence, i.e., a noncatalytic reaction path (Au electrode) and a catalytic reduction path (Sn electrode). The catalytic role of the electrode material surface in the electrolyte decomposition process demonstrated in this study may play a more general role in LIBs than heretofore recognized.

■ ASSOCIATED CONTENT

Supporting Information

Additional information about the *in situ* ATR-FTIR cell setup, experimental details, and reference compound solvation spectra. This material is available free of charge via the Internet at http://pubs.acs.org.

■ AUTHOR INFORMATION

Corresponding Authors

*somorjai@berkeley.edu (G.A.S.)
*kyriakos@me.berkeley.edu (K.K.)

Notes

The authors declare no competing financial interest.

■ ACKNOWLEDGMENTS

This work was supported by the Assistant Secretary for Energy Efficiency and Renewable Energy, Office of Freedom CAR and Vehicle Technologies of the U.S. Department of Energy under Contract No. DE-AC02 O5CH1123. The last author (K.K.) also acknowledges the funding provided for this work by the UCB–KAUST Academic Excellence Alliance (AEA) Program. The IR instrumentation was purchased with funding from the Director, Office of Basic Energy Sciences, Materials Science and Engineering Division of the U.S. Department of Energy.

■ REFERENCES

(1) Goodenough, J. B.; Park, K.-S. *J. Am. Chem. Soc.* **2013**, *135*, 1167.
(2) Peled, E. *J. Electrochem. Soc.* **1979**, *126*, 2047.
(3) Moshkovich, M.; Gofer, Y.; Aurbach, D. *J. Electrochem. Soc.* **2001**, *148*, E155.
(4) Aurbach, D.; Moshkovich, M.; Cohen, Y.; Schechter, A. *Langmuir* **1999**, *15*, 2947.
(5) Zhuang, G. V.; Yang, H.; Ross, P. N.; Xu, K.; Jow, T. R. *Electrochem. Solid-State Lett.* **2006**, *9*, A64.
(6) Verma, P.; Maire, P.; Novák, P. *Electrochim. Acta* **2010**, *55*, 6332.
(7) Xu, K.; Cresce, A. V. *J. Mater. Chem.* **2011**, *21*, 9849.
(8) Ross, P. N. *ECS Trans.* **2006**, *1*, 161.
(9) Aurbach, D. *J. Power Sources* **2000**, *89*, 206.
(10) Balbuena, P. B.; Wang, Y. *Lithium-Ion Batteries: Solid-Electrolyte Interphase*; Imperial College Press: London, 2004.
(11) Schroder, K. W.; Celio, H.; Webb, L. J.; Stevenson, K. J. *J. Phys. Chem. C* **2012**, *116*, 19737.
(12) Xu, K. *Chem. Rev.* **2004**, *104*, 4303.
(13) Tavassol, H.; Buthker, J. W.; Ferguson, G. A.; Curtiss, L. A.; Gewirth, A. A. *J. Electrochem. Soc.* **2012**, *159*, A730.
(14) Lucas, I. T.; Syzdek, J.; Kostecki, R. *Electrochem. Commun.* **2011**, *13*, 1271.
(15) Philippe, B.; Dedryvère, R.; Gorgoi, M.; Rensmo, H.; Gonbeau, D.; Edström, K. *J. Am. Chem. Soc.* **2013**, *135*, 9829.
(16) Ross, P. N. *Catal. Lett.* **2014**, *144*, 1370.
(17) Chen, Y.; Kanan, M. W. *J. Am. Chem. Soc.* **2012**, *134*, 1986.
(18) Beattie, S. D.; Hatchard, T.; Bonakdarpour, A.; Hewitt, K. C.; Dahn, J. R. *J. Electrochem. Soc.* **2003**, *150*, A701.
(19) Courtney, I. A.; Dahn, J. R. *J. Electrochem. Soc.* **1997**, *144*, 2405.
(20) Qiao, R.; Lucas, I. T.; Karim, A.; Syzdek, J.; Liu, X.; Chen, W.; Persson, K.; Kostecki, R.; Yang, W. *Adv. Mater. Interfaces* **2014**, *1*, 1300115.
(21) Aurbach, D. *J. Electrochem. Soc.* **1989**, *136*, 906.
(22) Akita, Y.; Segawa, M.; Munakata, H.; Kanamura, K. *J. Power Sources* **2013**, *239*, 175.
(23) Li, J.-T.; Chen, S.-R.; Ke, F.-S.; Wei, G.-Z.; Huang, L.; Sun, S.-G. *J. Electroanal. Chem.* **2010**, *649*, 171.
(24) Li, J.-T.; Chen, S.-R.; Fan, X.-Y.; Huang, L.; Sun, S.-G. *Langmuir* **2007**, *23*, 13174.
(25) Zhuang, G. V.; Xu, K.; Yang, H.; Jow, T. R.; Ross, P. N. *J. Phys. Chem. B* **2005**, *109*, 17567.
(26) Shi, F.; Zhao, H.; Liu, G.; Ross, P. N.; Somorjai, G. A.; Komvopoulos, K. *J. Phys. Chem. C* **2014**, *118*, 14732.
(27) Song, S.-W.; Zhuang, G. V.; Ross, P. N. *J. Electrochem. Soc.* **2004**, *151*, A1162.
(28) Tasaki, K.; Harris, S. J. *J. Phys. Chem. C* **2010**, *114*, 8076.
(29) Tasaki, K.; Goldberg, A.; Lian, J.-J.; Walker, M.; Timmons, A.; Harris, S. J. *J. Electrochem. Soc.* **2009**, *156*, A1019.
(30) Wang, Y.; Nakamura, S.; Ue, M.; Balbuena, P. B. *J. Am. Chem. Soc.* **2001**, *123*, 11708.
(31) Zhuang, G. V.; Yang, H.; Blizanac, B.; Ross, P. N. *Electrochem. Solid-State Lett.* **2005**, *8*, A441.
(32) Yoshida, H.; Fukunaga, T.; Hazama, T.; Terasaki, M.; Mizutani, M.; Yamachi, M. *J. Power Sources* **1997**, *68*, 311.
(33) Sasaki, T.; Abe, T.; Iriyama, Y.; Inaba, M.; Ogumi, Z. *J. Power Sources* **2005**, *150*, 208.
(34) Gachota, G.; Grugeon, S.; Armand, M.; Pilard, S.; Guenot, P.; Tarascon, J.-M.; Laruelle, S. *J. Power Sources* **2008**, *178*, 409.
(35) Sasaki, T.; Abe, T.; Iriyama, Y.; Inaba, M.; Ogumi, Z. *J. Electrochem. Soc.* **2005**, *152*, A2046.

DOI: 10.1021/ja5128456
J. Am. Chem. Soc. 2015, 137, 3181–3184